Available online at www.sciencedirect.com

ScienceDirect

Mendeleev Commun., 2021, **31**, 459–461

Mendeleev Communications

Effect of contact barrier heights on the power conversion efficiency of a perovskite photovoltaic element

Yaroslav B. Martynov,*[a] Rashid G. Nazmitdinov,[b,c] Pavel P. Gladyshev[c] and Andrea Moià-Pol[d]

[a] *State Scientific-Production Enterprise 'Istok', 141190 Fryazino, Moscow Region, Russian Federation. E-mail: yaroslavmartynov@yandex.ru*
[b] *Joint Institute for Nuclear Research, 141980 Dubna, Moscow Region, Russian Federation*
[c] *Dubna University, 141982 Dubna, Moscow Region, Russian Federation*
[d] *Universitat de les Illes Balears, E-07122 Palma de Mallorca, Spain*

DOI: 10.1016/j.mencom.2021.07.007

The influence of contact barrier heights on the principal characteristics (open circuit voltage, short circuit current, fill factor, and power conversion efficiency) of a perovskite photovoltaic element was examined by numerical simulations in order to reach a maximum efficiency of the element. The role of crystal fields at the perovskite boundaries was pointed out.

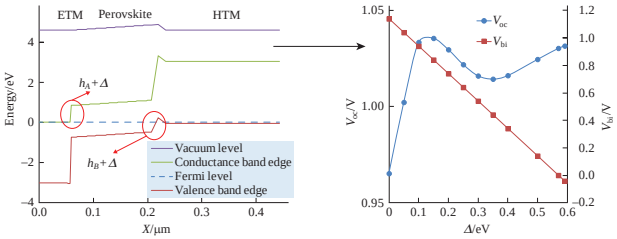

Keywords: perovskite photovoltaic element, numerical simulation, power conversion efficiency limit, structure optimization.

Rapid progress in the efficiency of photovoltaic elements based on hybrid organic–inorganic perovskites attracts a tremendous experimental and theoretical attention[1]. The instability of the first photovoltaic elements was gradually overcome either by simply encapsulating the sensitive parts[2] and creating hydrophobic contacts[3] or by replacing conventional perovskites with stable modifications.[4] In particular, a power conversion efficiency (PCE) of around 25% was reported.[5] The Shockley–Queisser efficiency limit of perovskite solar cells with a perovskite band gap of 1.58 eV is about 31% under standard conditions AM1.5G.[6] The formation of morphology contacts to perovskite for suppressing interface charge recombination was studied.[7–11] The careful treatment of band offsets at perovskite–electron transport material (ETM) and perovskite–hole transport material (HTM) interfaces is also important. Much attention is paid to the lowering of barriers that prohibit the extraction of current carriers from the absorber.[12] At the same time, the barriers to the current flow from ETM/HTM layers to the absorber play a significant role.[13–15] Here, we consider the typical architecture of a perovskite photovoltaic element (PPE) as an example: TiO_2–$CH_3NH_3PbI_3$–Spiro-OMeTAD. The PCE of the PPE can be further improved by tailoring contact barrier heights.

The PCE of the PPE can be expressed as $J_{sc}V_{oc}FF/P_{inc}$, where J_{sc} is the short circuit current; V_{oc} is the open circuit voltage; FF is a fill factor, and P_{inc} is the solar irradiation power. To increase the J_{sc}, a sufficiently thick absorber or light-trapping mechanisms should be used. On the other hand, the product (V_{oc}FF in p–i–n or p–n photodiode is the increasing function, when the total recombination rate R decreases. The rate R can be defined as

$$R = N_{mean} L_A/\tau_{lf}, \quad (1)$$

where N_{mean} is the mean (over absorber thickness) injected carrier concentration, τ_{lf} is the carrier recombination lifetime, and L_A is the absorber thickness. Consequently, a decrease in the absorber thickness increases the product V_{oc}FF. At the same time, the decrease in the thickness should decrease the short circuit current. Since we can keep J_{sc} nearly constant with the aid of a light-trapping technique, it follows from (1) that the PCE increases with (*a*) absorber purification due to an increase of the carrier life time τ_{lf},[16] (*b*) decreasing the absorber thickness,[17] and (*c*) tailoring contact barriers to decrease the carrier concentration injected into the absorber N_{mean}. The influence of τ_{lf} and L_A on the PCE of the PPE was investigated previously,[16,17] and we will consider the contact tailoring.

Let us discuss the influence of recombination on the product V_{oc}FF and consider the band structure of a typical TiO_2–$CH_3NH_3PbI_3$–Spiro-OMeTAD PPE [Figure 1(*a*)]. It is well known that a maximum voltage is obtained under the illumination of a photovoltaic element under open circuit conditions. This voltage shifts a p–i–n diode in the forward direction and generates the injection of electrons from TiO_2 and holes from Spiro-OMeTAD into the perovskite. This injection current (j) should be precisely equal to the

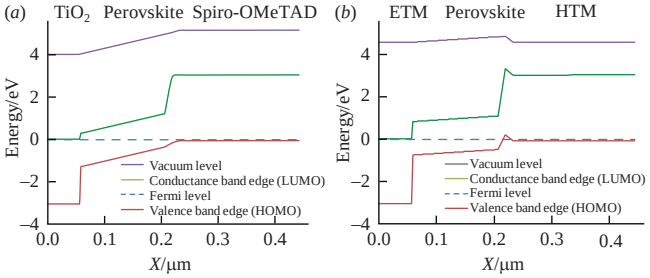

Figure 1 The p–i–n band structures of (*a*) the initial PPE TiO_2–$CH_3NH_3PbI_3$–Spiro-OMeTAD, V_{bi} = 1.14 V and (*b*) the modified diodes, V_{bi} = 0.

photogenerated current flowing in the opposite direction (J_{sc}). We recall that the current (j) is

$$j = j_s\left(e^{\frac{qV}{kT}} - 1\right), \quad (2)$$

where k is the Boltzmann constant, q is the electron charge modulus, T is the absorber lattice temperature, and j_s is the injection current at high negative applied voltages $V \to -\infty$. At $V = V_{oc}$, the total current through the irradiated PPE is $j_T = j(V_{oc}) - J_{sc} = 0$; consequently, we have

$$V_{oc} = \frac{kT}{q}\ln(J_{sc}/j_s + 1). \quad (3)$$

From the continuity equation for the perovskite layer of the PPE in the dark at a high reverse bias, it follows that

$$\frac{\partial j_n}{\partial x} = q\frac{np - n_i^2}{\tau_{lf}(n + p)}. \quad (4)$$

Here, j_n is the electron current through the diode; n, p are the electron and hole densities, respectively; and n_i is the carrier density in the intrinsic semiconductor. Using (4), we obtain

$$j_n(A) = j_n(B) = qN_{mean}L_A/\tau_{lf}, \quad (5)$$

where $j_n(A)$, $j_n(B)$ are the values of j_n at the TiO_2–perovskite and perovskite–Spiro-OMeTAD interfaces, respectively; while the mean injected carrier concentration is

$$N_{mean} = \frac{1}{L_A}\int_0^{L_A}\frac{np - n_i^2}{(n + p)}dx. \quad (6)$$

There is a very high barrier for electrons flowing in the forward direction at the perovskite–Spiro-OMeTAD interface (Figure 1). Consequently, the electron current to the right from this boundary is zero; hence, $j_n(B) = 0$. Similarly, there is a very high barrier for the holes moving in the forward direction at the perovskite–TiO_2 interface. Consequently, the hole current to the left from this boundary is zero; hence, $j_n(A) = j_s$ and

$$j_s = qN_{mean}L_A/\tau_{lf}. \quad (7)$$

Combining (3) and (7), we obtain

$$V_{oc} = \frac{kT}{q}\ln\left(\frac{J_{sc}\tau_{lf}}{qN_{mean}L_A} + 1\right). \quad (8)$$

Next, we attempt to reduce the injected carrier concentration N_{mean} by increasing the heights of two barriers. The first barrier is located on the left perovskite boundary ($h_A = \chi_A - \chi_P$). It prohibits the forward electron current flow or the injection of electrons to the perovskite. The second one is located on the right perovskite boundary ($h_B = \chi_P + E_{gP} - \chi_B - E_{gB}$). It prohibits the forward hole current flow or the injection of holes to the perovskite. Here, χ_A, χ_B, χ_P are the electron affinities of the ETM, HTM, and perovskite, respectively; and E_{gP}, E_{gB} are the perovskite and the HTM band gaps, respectively. The barrier height h_A can be increased if we replace TiO_2 by a semiconductor with higher electron affinity $\tilde{\chi}_A = \chi_A + \Delta_A$, and, hence, $\tilde{h}_A = h_A + \Delta_A$. The barrier height h_B can be increased if we replace Spiro-OMeTAD by a semiconductor with lower electron affinity $\tilde{\chi}_B = \chi_B + \Delta_B$ and, hence, $\tilde{h}_B = h_B + \Delta_B$ (see Figure 1). Note that the electric fields generated by the built-in voltage (V_{bi}) and the crystal electric field generated by band discontinuities at the interfaces can contribute to the photogenerated electron–hole separation. Therefore, we vary the heights of these barriers simultaneously $\Delta_A = \Delta_B \equiv \Delta$ with all other band parameters remain unchanged. This procedure keeps the sum

$$V_S = \tilde{V}_{bi} + \tilde{h}_A + \tilde{h}_B = \text{const}. \quad (9)$$

Here, the voltage $\tilde{V}_{bi}$ is the built-in voltage

$$\tilde{V}_{bi} = W_B - W_A, \quad (10)$$

and W_A, W_B are the working functions of the ETM and HTM, respectively:

$$W_A = \tilde{\chi}_A + kT\ln\left(\frac{N_C}{n_n}\right), \quad (11)$$

$$W_B = \tilde{\chi}_B + E_{gB} - kT\ln\left(\frac{N_V}{p_p}\right),$$

$$N_C = 2\left(\frac{2\pi m_n^* kT}{h^2}\right)^{\frac{3}{2}},$$

$$N_V = 2\left(\frac{2\pi m_p^* kT}{h^2}\right)^{\frac{3}{2}}.$$

m_n^*/m_p^* are electron/hole effective masses in ETM/HTM, respectively; h is the Plank constant; n_n, p_p are the main carrier concentrations in the ETM and HTM, respectively. Since we assume the ETM donor doping $N_D = 10^{19}$ cm^{-3} and the HTM acceptor doping $N_A = 3 \times 10^{18}$ cm^{-3}, $n_n \approx N_D$ and $p_p \approx N_A$. Expressions (10) and (11) indicate that the built-in voltage decreases with Δ: $\tilde{V}_{bi} = V_{bi} - 2\Delta$.

Initial barrier heights for TiO_2–$CH_3NH_3PbI_3$–Spiro-OMeTAD are $h_A = 0.25$ eV and $h_B = 0.11$ eV. With simultaneously increasing the heights of these barriers by adding portions (Δ) to the ETM and HTM electron affinities, we calculated the PCE for the resulting PPE structure. The initial structure of a TiO_2–$CH_3NH_3PbI_3$–Spiro-OMeTAD p–i–n diode has the built-in voltage $V_{bi} = 1.14$ V [Figure 1(*a*)]. It was gradually modified by the above process to the p–i–n structure with a zero built-in voltage [Figure 1(*b*)].

The calculations demonstrate that a decrease in the forward injection current (and N_{mean}) with the height of barriers leads to the expected increase of the open circuit voltage [Figure 2(*a*)]. Then, this growth is replaced by a small drop of V_{oc} at $\Delta \sim 0.35$ eV, and the voltage V_{oc} finally increases again. The PCE of the PPE has a maximum at $\Delta = 0.2$ eV ($\tilde{h}_A = 0.45$ eV; $\tilde{h}_B = 0.31$ eV) [Figure 2(*b*)] due to poor FFs for the devices with $\Delta > 0.3$ eV [Figure 3(*a*)]. According to the calculations, the optimal PPE structure is approached under the following conditions: the ETM with the electron affinity $\tilde{\chi}_A = 4.2$ eV and a band gap of 3.05 eV; the perovskite with electron affinity of 3.75 eV and $E_{gP} = 1.58$ eV; and the HTM with the electron affinity $\tilde{\chi}_B = 1.92$ eV and $E_{gB} = 3.1$ eV. Such a small shift in TiO_2 conduction band energy, for example, can be obtained by $TiCl_4$ treatment on the compact TiO_2 layer.[13] The short circuit current is almost constant at the various values of Δ [Figure 3(*b*)]. This current remains unchanged even at $\Delta = 0.57$ eV when $\tilde{V}_{bi} = 0$. This fact indicates that strong crystal fields at the perovskite boundaries are sufficient for the separation of photogenerated electrons and holes at a constant sum V_S. Note that, even at $\Delta = 0.57$ eV, a small electric field still exists inside the absorber

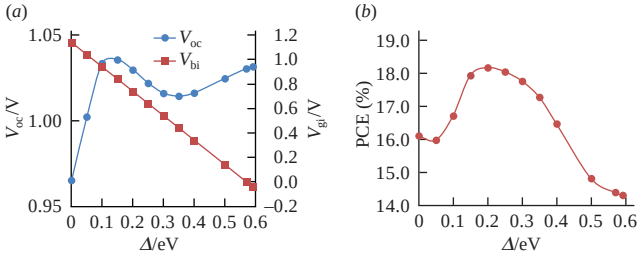

Figure 2 (*a*) Open circuit and built-in voltages and (*b*) the PCE as functions of the barrier height increments.

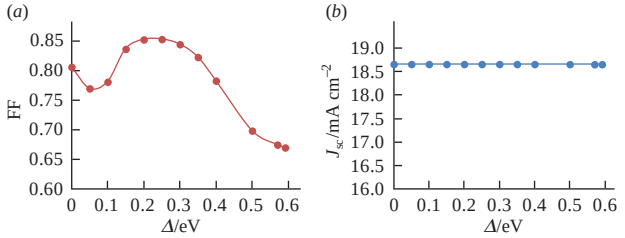

Figure 3 (*a*) FF and (*b*) the short circuit current as functions of the barrier height increments.

due to the suppressed but nonzero tails of the injected electrons and holes [see Figure 1(*b*)].

The engineering of different layer interfaces in perovskite solar cells is of considerable current interest.[13–15] In particular, the ETM-perovskite barrier height was increased from 0.2 to ~0.5 eV by $TiCl_4$ treatment on the compact TiO_2 layer in planar PSCs[13]. It results in an increase of the V_{oc} and PCE. Furthermore, a new family of 2D transition metal carbides, nitrides and carbonitrides (MXenes) opens a new avenue in the interface engineering. For example, the height of the ETM–perovskite barrier can be varied from 0.45 to 0.05 eV by including MXenes as a dopant or an interlayer.[14] It was observed that the initial rise of the open circuit voltage V_{oc} and the PCE of the corresponding PSC were followed by a rapid decrease. This result is in a qualitative agreement with the optimal barrier height found in our research. The discrepancies can arise from the fact that the above treatments[13,14] affect the ETM–perovskite band alignments and additionally increase the short circuit current. The latter implies the change of the number of additional interfacial vacancies and defects that are equal to the volume values in our model. This requirement corresponds to the ideal contact conditions that can occur in well-constructed structures.[18]

Thus, the PCE of a perovskite photovoltaic element can be further improved by tailoring the contact barrier height, which can be an additional independent approach to well-known methods such as the purification of a perovskite crystal structure or the use of light-trapping mechanisms.

References

1 P. P. Gladyshev, M. Banavoth, T. Swetha, N. Bingwa, Ya. B. Martynov, T. Yu. Zelenyak, V. A. Kinev and R. G. Nazmitdinov, in *Perovskite Solar Cells: Properties, Application and Efficiency*, ed. M. Banavoth, Nova Science Publishers, 2019, pp. 1–76.
2 F. Matteocci, L. Cinà, E. Lamanna, S. Cacovich, G. Divitini, P. A. Midgley, C. Ducati and A. Di Carlo, *Nano Energy*, 2016, **30**, 162.
3 S. Gholipour, J.-P. Correa-Baena, K. Domanski, T. Matsui, L. Steier, F. Giordano, F. Tajabadi, W. Tress, M. Saliba, A. Abate, A. M. Ali, N. Taghavinia, M. Grätzel and A. Hagfeldt, *Adv. Energy Mater.*, 2016, **6**, 1601116.
4 E. I. Marchenko, S. A. Fateev, A. A. Petrov, E. A. Goodilin and A. B. Tarasov, *Mendeleev Commun.*, 2020, **30**, 279.
5 J. J. Yoo, G. Seo, M. R. Chua, T. G. Park, Y. Lu, F. Rotermund, Y.-K. Kim, C. S. Moon, N. J. Jeon, J.-P. Correa-Baena, V. Bulović, S. S. Shin, M. G. Bawendi and J. Seo, *Nature*, 2021, **590**, 587.
6 A. Dualeh, N. Tétreault, T. Moehl, P. Gao, M. K. Nazeeruddin and M. Grätzel, *Adv. Funct. Mater.*, 2014, **24**, 3250.
7 B. Yang, O. Dyck, J. Poplawsky, J. Keum, A. Puretzky, S. Das, I. N. Ivanov, C. M. Rouleau, G. Duscher, D. B. Geohegan and K. Xiao, *J. Am. Chem. Soc*., 2015, **137**, 29, 9210.
8 G. E. Eperon, V. M. Burlakov, P. Docampo, A. Goriely and H. J. Snaith, *Adv. Funct. Mater.*, 2014, **24**, 151.
9 W. S. Yang, B.-W. Park, E. H. Jung, N. J. Jeon, Y. C. Kim, D. U. Lee, S. S. Shin, J. Seo, E. K. Kim, J. H. Noh and S. I. Seok, *Science*, 2017, **356**, 1376.
10 H. Zhou, Q. Chen, G. Li, S. Luo, T. Song, H.-S. Duan, Z. Hong, J. You, Y. Liu and Y. Yang, *Science*, 2014, **345**, 542.
11 A. B. Nikolskaia, M. F. Vildanova, S. S. Kozlov and O. I. Shevaleevskiy, *Russ. Chem. Bull., Int. Ed.*, 2020, **69**, 1245 (*Izv. Akad. Nauk, Ser. Khim.*, 2020, 1245).
12 P. M. Sokolov, M. A. Zvaigzne, V. A. Krivenkov, A. P. Litvin, A. V. Baranov, A. V. Fedorov, P. S. Samokhvalov and I. R. Nabiev, *Russ. Chem. Rev.*, 2019, **88**, 370.
13 Y. Xu, C. Gao, S. Tang, J. Zhang, Y. Chen, Y. Zhu and Z. Hu, *J. Alloys Compd.*, 2019, **787**, 1082.
14 A. Agresti, A. Pazniak, S. Pescetelli, A. Di Vito, D. Rossi, A. Pecchia, M. A. der Maur, A. Liedl, R. Larciprete, D. V. Kuznetsov, D. Saranin and A. Di Carlo, *Nat. Mater.*, 2019, **18**, 1228.
15 S. Wang, T. Sakurai, W. Wen and Y. Qi, *Adv. Mater. Interfaces*, 2018, **5**, 1800260.
16 Y. B. Martynov, R. G. Nazmitdinov, A. Moià-Pol, P. P. Gladyshev, A. R. Tameev, A. V. Vannikov and M. Pudlak, *Phys. Chem. Chem. Phys.*, 2017, **19**, 19916.
17 F. Bonnín-Ripoll, Y. B. Martynov, G. Cardona, R. G. Nazmitdinov and R. Pujol-Nadal, *Sol. Energy Mater. Sol. Cells*, 2019, **200**, 110050.
18 B. Yang, O. Dyck, J. Poplawsky, J. Keum, A. Puretzky, S. Das, I. Ivanov, C. Rouleau, G. Duscher, D. Geohegan and K. Xiao, *J. Am. Chem. Soc*., 2015, **137**, 9210.

Received: 1st March 2021; Com. 21/6469